Observation of Spatial Inhomogeneities in *N-tert*-Butylbenzothiazolesulfenamide–Sulfur Cured High-Vinyl Polybutadiene Using NMR Imaging

M. A. Rana and J. L. Koenig*

Department of Macromolecular Science, Case Western Reserve University, 10900 Euclid Avenue, Cleveland, Ohio 44106-7202

Received August 24, 1993; Revised Manuscript Received February 22, 1994®

ABSTRACT: Proton nuclear magnetic resonance imaging (NMRI) was used to study the different physical and spatial microstructures present in an unfilled accelerated–sulfur cured high-vinyl polybutadiene material. Samples of different formulations were cured at 150 °C from 20 to 120 min in order to monitor the changes associated with the cure times. Voids and other inhomogeneities were detected on the basis of magnetic susceptibility differences. A solvent imaging method using cyclohexane was used to probe the different morphological defects. Reversion, a process involving a decrease in the overall cross-link density, was observed in the samples cured for 120 min. Sample morphological features as small as 0.07 mm can be detected.

Introduction

Flourishing in the field of medicine,[1,2] nuclear magnetic resonance imaging (NMRI) is also recognized as an important tool in the area of materials research. The NMRI is extensively used to study the chemical and motional heterogeneities in the cross-linked elastomeric networks because of their greater segmental mobility and large extensibility when swollen in an appropriate solvent.[3-5] The image provides a picture of NMR signal intensity as a function of location (in one, two, and three dimensions) in an object. The main advantage of this technique over the other imaging methods is its ability to map spatially a wide variety of structures, both static and dynamic parameters, in a noninvasive way.[6]

Until recently the only techniques available to study spatial microstructures required sectioning the sample and analyzing the resulting slice by using different methods such as scanning electron microscopy (SEM), infrared spectroscopy (IR), and electron spectroscopy (ESCA). In certain cases X-ray tomography has also been used to study the cured microstructures.[7,8]

NMR imaging involves acquiring the NMR spectra in the presence of large magnetic field gradients in the x, y, and z directions. One gradient is used in conjunction with a selective pulse to excite spins only in a slice of the sample, while the other two gradients spatially encode the spins so that the resonant frequencies of the nuclear spins are correlated with spatial position. A two-dimensional (2D) Fourier transform is performed after collecting the data. Thus a 2D image is a plot of intensity vs spatial direction. The images produced by this technique are determined by optimizing various parameters. Extrinsic parameters include operator-controlled parameters such as field strength, radio-frequency pulses, and pulse sequence timings, whereas the intrinsic parameters are the proton spin density ρ, spin–lattice relaxation time (T_1), spin–spin relaxation time (T_2), chemical shift, and flow velocity. Thus a signal intensity is a complex interplay of these various parameters. A good quality image can be acquired if these parameters are well controlled and optimized.

The spatial mapping and contrast capabilities of NMRI have created natural incentives for exploiting NMRI in the field of elastomers[9-24] and solid samples.[25-27] For the study of the molecular mobility of the polymer chains, the

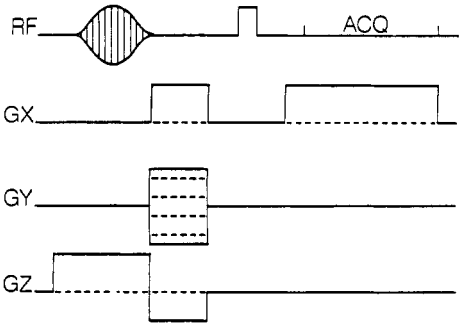

Figure 1. Block diagram of the Carr–Purcell spin-echo pulse sequence. Slice selection is accomplished with the selective 90° pulse and the G_z gradient, while the G_x gradient is the frequency encoding and read gradient and the G_y is the phase encoding gradient.

NMRI technique provides a sensitive probe of the nuclear environment through the short-range magnetic dipolar interactions.[28] The variety of characteristic motions can be interpreted in terms of relaxation parameters which include spin–lattice relaxations time (T_1), sensitive to group motions in the megahertz frequency regime. The motions inducing the spin–spin relaxation (T_2) are in the kilohertz range and are sensitive to chain mobility.

The detection of internal voids, defects, and inhomogeneities constitutes an important class of applications for NMRI. This category of morphological investigation typically relies on the NMR signal acquired from a protic solvent imbibed in the sample.

The goal of this study has been to evolve a better understanding of structure/property relationships in an accelerated–sulfur vulcanized high-vinyl polybutadiene rubber (BR). Both imbibed solvent (cyclohexane) and direct proton imaging (deuterated cyclohexane) approaches have been evaluated.

Experimental Section

The elastomeric sample under investigation is high vinyl BR a product of Nippon Zeon Co., Ltd., sold under the commercial name of Nipol BR-1245. This system has approximately 70% of the vinyl 1,2 units, and the rest (30%) comprises of 1,4 BR units. The samples were blended on a Brabender mixer and formulated to different accelerator to sulfur ratios along with the other auxiliary agents (e.g., zinc oxide and stearic acid). The formulated rubber samples consisted of 100 phr (parts per hundred of rubber) of Nipol BR-1245 rubber, and the other

® Abstract published in *Advance ACS Abstracts,* May 15, 1994.

0024-9297/94/2227-3727$04.50/0

Table 1. Equilibrium Swelling Measurement Data for Conventional Formulation

	cure time (min)				
	20.00	35.00	45.00	60.00	120.00
vol. fraction of rubber V_r	0.238	0.239	0.239	0.238	0.267
ν (swelling) (10^{-4})	1.25	1.22	1.31	1.42	1.64
$M_{n,phys}$ (10^4)	0.42	0.41	0.38	0.35	0.30
av monomer units/nodal junction	77.0	75.0	70.0	65.0	56.0
Kraus' Correction					
$M_{n,phys}$ (10^4)	0.40	0.38	0.36	0.33	0.29
$M_{n,chem}$ (10^4)	0.21	0.20	0.19	0.17	0.15
ave monomer units/nodal junction	73.0	71.0	66.0	62.0	54.0

standard deviation: ± 0.011

Table 2. Equilibrium Swelling Measurement Data for Semiefficient Formulation

	cure time (min)				
	20.00	35.00	45.00	60.00	120.00
vol. fraction of rubber V_r	0.192	0.222	0.220	0.238	0.226
ν (swelling) (10^{-4})	1.04	1.11	1.21	1.33	1.43
$M_{n,phys}$ (10^4)	0.48	0.45	0.43	0.38	0.35
av monomer units/nodal junction	89.0	83.0	79.0	70.0	65.0
Kraus' Correction					
$M_{n,phys}$ (10^4)	0.45	0.42	0.40	0.36	0.33
$M_{n,chem}$ (10^4)	0.24	0.22	0.21	0.19	0.17
av monomer units/nodal junction	82.0	78.0	75.0	66.0	61.0

standard deviation: ±0.015

components include 4.1, 2.0, and 1.1 phr of elemental sulfur and 0.8, 2.0, and 5.0 phr of *N-tert*-butylbenzothiazolesulfenamide (TBBS) for conventional (conv), semiefficient (sev), and efficient (ev) formulation, respectively. The accelerator contributes to a relatively longer induction period and a faster cure rate (a product of Monsanto Corp.).

Table 3. Equilibrium Swelling Measurement Data for Efficient Formulation

	cure time (min)				
	20.00	35.00	45.00	60.00	120.00
vol. fraction rubber V_r	0.275	0.238	0.216	0.232	0.241
ν (swelling) (10^{-4})	1.00	1.09	1.22	1.43	1.70
$M_{n,phys}$ (10^4)	0.50	0.46	0.41	0.35	0.29
av monomer units/nodal junction	92.0	84.0	76.0	65.0	54.0
Kraus' Correction					
$M_{n,phys}$ (10^4)	0.46	0.42	0.38	0.33	0.28
$M_{n,chem}$ (10^4)	0.25	0.23	0.20	0.17	0.15
av monomer units/nodal junction	86.0	79.0	71.0	61.0	52.0

standard deviation: ±0.019

The formulated samples were cured at 150 °C, forming a rubber sheet (1 mm thick) on a hydraulic press using a pressure of 2000 psi for different lengths of times. These rubber sheets were cured from 20 to 120 min in order to monitor the changes associated with the cure as a function of cure time. These cured samples were immediately quenched by immersing in a powdered bed of dry ice. The samples were later extracted with cyclohexane overnight in a Soxhlet extractor in order to remove the non-network materials. All these samples were stored in a refrigerator in cyclohexane to avoid degradation.

The equilibrium swelling method was used in order to measure the cross-link densities. All the studies were made at ambient temperature using cyclohexane as a swelling solvent. The number-average (M_n) and weight-average (M_w) molecular weights of unfilled original BR material were determined by using the

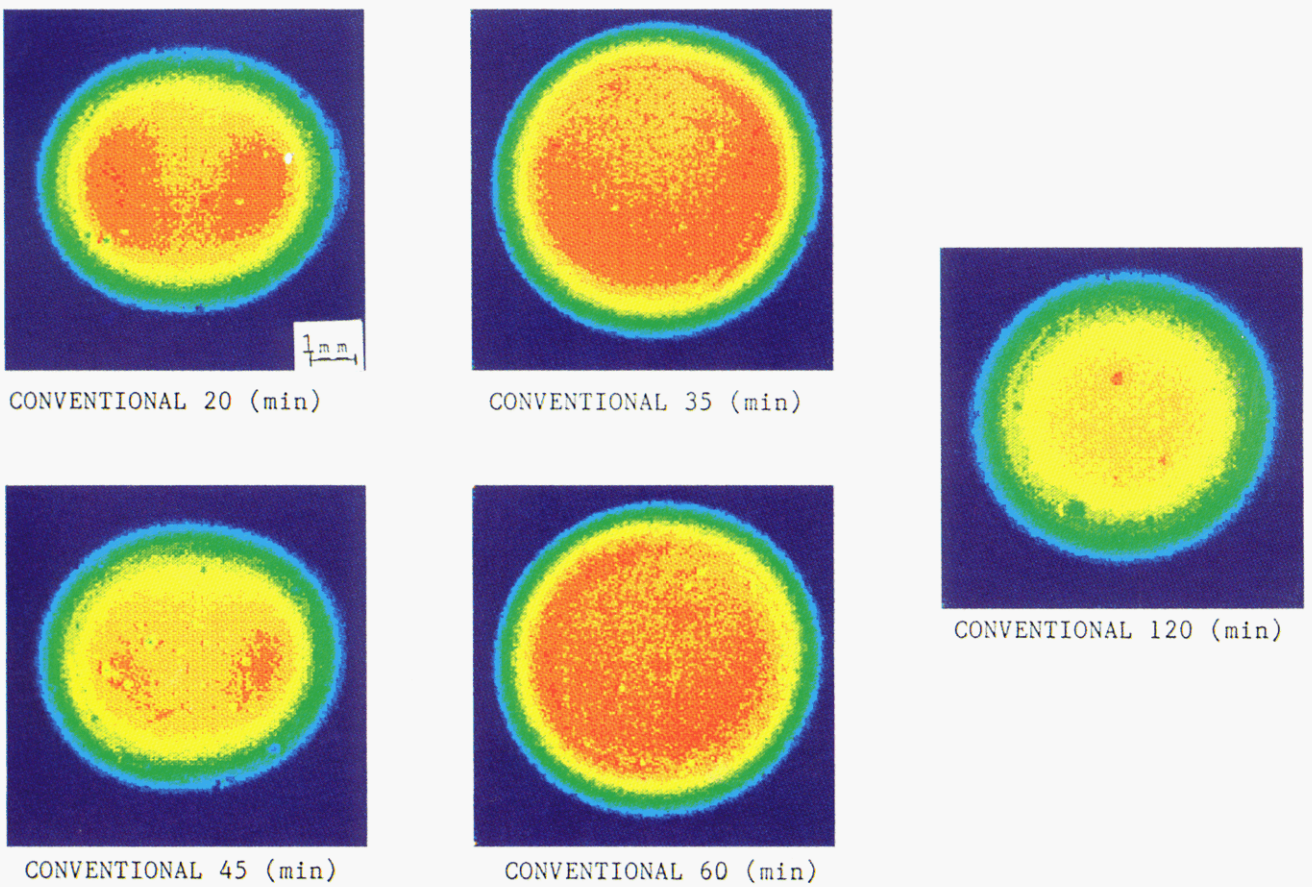

Figure 2. Proton image of a high-vinyl polybutadiene cured sample swollen in cyclohexane using spin-echo pulse sequence. FOV = 9 × 9 mm displayed as 256 × 256 pixels. The effective pixel resolution is 39 μm/pixel. (a) 20 min; (b) 35 min; (c) 45 min; (d) 60 min; (e) 120 min cured (conventional formulation).

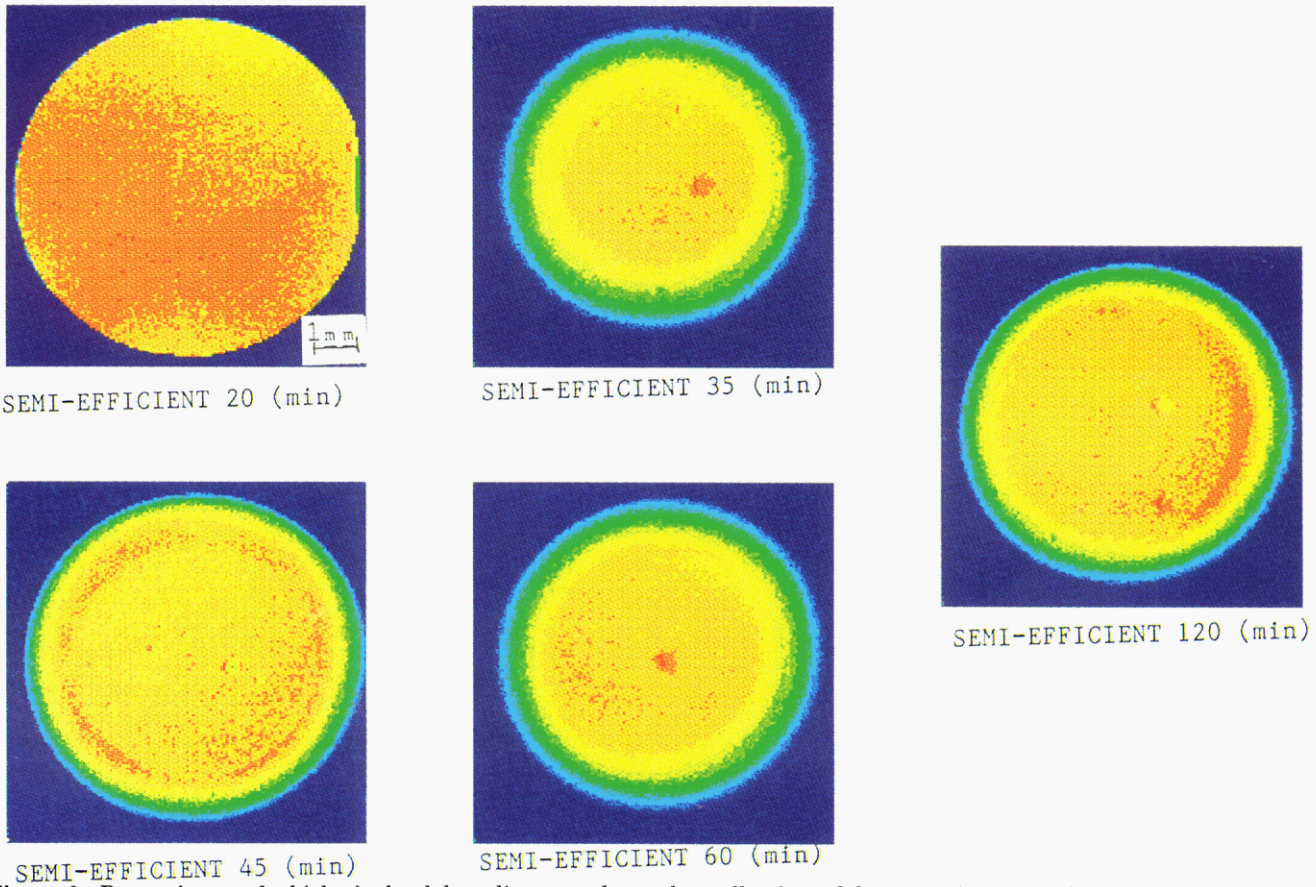

Figure 3. Proton image of a high-vinyl polybutadiene cured sample swollen in cyclohexane using spin-echo pulse sequence. FOV = 9 × 9 mm displayed as 256 × 256 pixels. The effective pixel resolution is 39 μm/pixel. (a) 20 min; (b) 35 min; (c) 45 min; (d) 60 min; (e) 120 min cured (semiefficient formulation).

GPC method. The average M_n and M_w calculated for original BR were 13 6000 and 14 600, respectively, with the polydispersity value of approximately 1.07.

A Bruker MSL-300 NMR spectrometer equipped with a microimaging probe was used to acquire the images at a proton frequency of 300.13 MHz. All these images were taken at 300 K. The cured samples were swollen both in *n*-cyclohexane and in deuterated cyclohexane in a 20-mm tube for 48 h prior to the experiment. The resulting images were displayed as 256 × 256 pixels in size.

The pulse sequence used was a standard CPMG (Carr–Purcell, Meiboom–Gill)[29,30] spin echo with a selective 90° pulse followed by a delay time τ. The nonselective 180° pulse is applied by another delay $T\delta$ and then the signal is acquired. The pulse sequence diagram is shown in Figure 1. The slice thickness was approximately 1 mm and was performed by using a magnetic field gradient in the *z*-direction during the selective 90° pulse. The images were acquired using an echo time of 7 ms and a repetition time of 5 s. A spectral width of 62 500 Hz was used in the acquisition.

Sixteen scans per phase encoding steps were signal averaged in producing each image, using 90° increment $(x, -y, -x, y)$ phase cycling. The read-out gradient was set as 19.80 G/cm, and the phase encode gradient varied between −16.25 and +16.25 G/cm in equal 256 increments of 0.13 G/cm.

The T_1 images were taken using the saturation recovery pulse sequence. The echo time (T_E) used was 5.75 ms, while the repetition time ranges from 10 ms to 5 s. The read-out gradient was set at 19.80 G/cm, while the phase encoding gradient varied between −16.25 and +16.25 G/cm in equal 256 increments of 0.14 G/cm. Twelve scans per phase encoding steps were signal averaged in producing each image.

The second set of samples were swollen in deuterated cyclohexane in order to image the rubber material directly. Sixteen scans per phase encoding step were signal averaged in producing each image. The echo time was 7 ms, while the repetition time was 5 s. The read-out gradient was set at 23.30 G/cm, while the phase encoding gradient varied between −19.20 and +19.20 G/cm in 256 equal increments of 0.15 G/cm. The images are displayed on the arbitrary scale of 0–255, which corresponds to from blue (low) to red (red) intensities, where 0 corresponds to the lowest signal intensity and 255 to the highest signal intensity. The other colors represent intensities between these extremes.

Results

The signal intensity in proton imaging depends on the proton concentration and T_1 and T_2 relaxation times. The spin-echo signal intensity increases if T_2 increases, T_1 decreases, or T_E is shortened. In the case of a cured rubber which acts as a pseudosolid, the images were hampered by the problem of excessive line widths and poor signal-to-noise ratios. The experimental criterion for generating a high-resolution NMR image is that it must be possible to encode spatial information in an NMR signal in a time order of T_2, the relaxation time.

Swelling measurements have been used for the determination of the cross-link density in elastomers.[31–33] The method is based on the fact that the higher the cross-link density, the less solvent is imbibed in the system and the lower the degree of swelling and vice versa. The results of equilibrium swelling measurements of differently cured high-vinyl polybutadiene are shown in Tables 1–3. These studies were made at ambient temperature using cyclohexane as a swelling solvent.

The number-average molecular weight between the physical cross-links ($M_{n,phys}$) was derived by using the Flory–Rehner equation.[31]

$$1/M_{n,phys} = \vartheta = \frac{-[\ln(1 - v_r) + v_r + \chi v_r^2]}{\rho_r v_0 (v_r^{1/3} - v_r/2)}$$

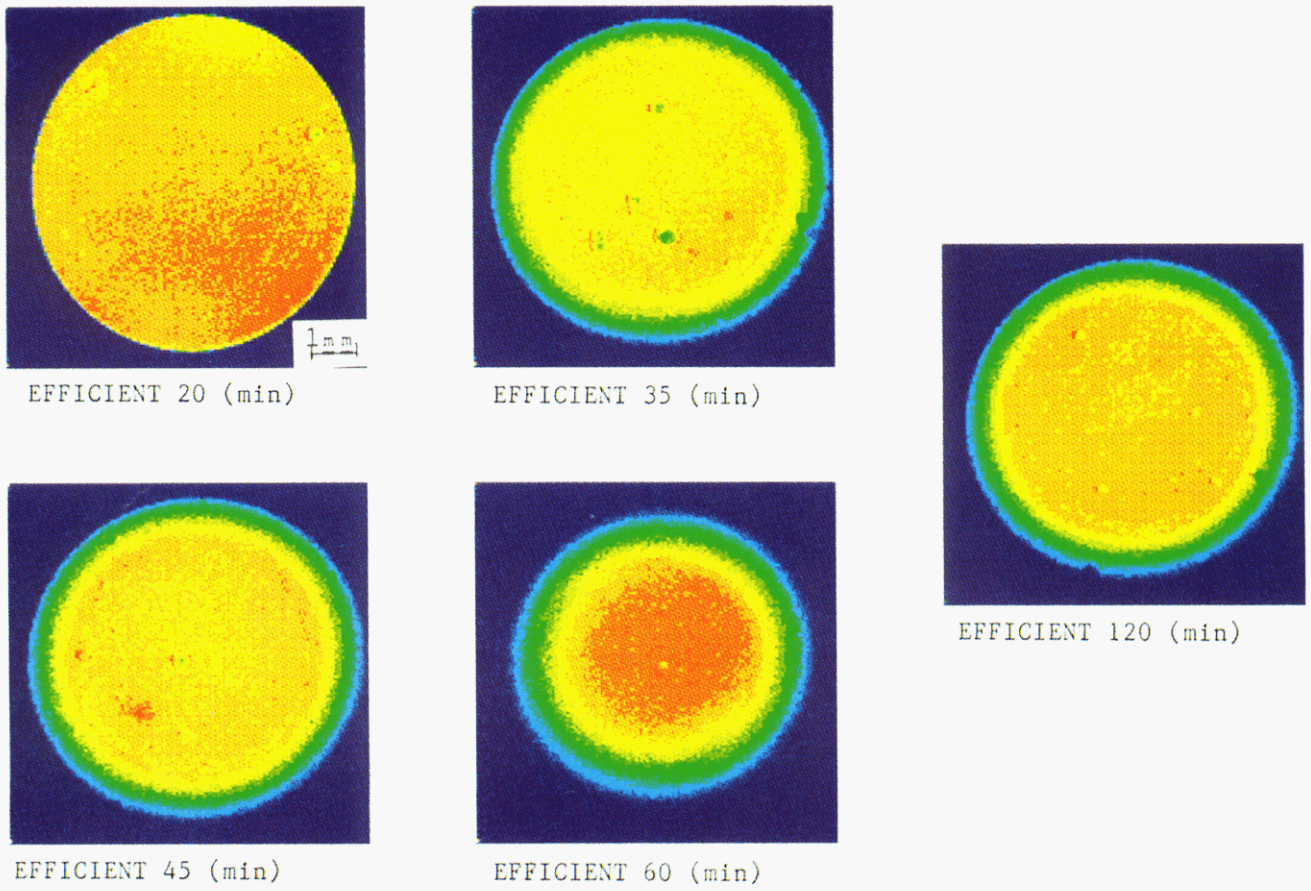

Figure 4. Proton image of a high-vinyl polybutadiene cured sample swollen in cyclohexane using spin-echo pulse sequence. FOV = 9 × 9 mm displayed as 256 × 256 pixels. The effective pixel resolution is 39 μm/pixel. (a) 20 min; (b) 35 min; (c) 45 min; (d) 60 min; (e) 120 min cured (efficient formulation).

The χ value is solvent–polymer interaction parameters characteristic of the interaction between the solvent system and the cured solid. The lower the χ value, the greater the solvent will swell the cross-linked polymer.

$$v_r = [(\rho_r/\rho_s)(W_s - W_u/W_u) + 1]^{-1}$$

$$\chi = 0.37 + 0.52v_r$$

where χ is evaluated for each sample as a linear function of v_r as shown in the above equation. Tables 1–3 show the average number of monomer units between the cross-links. These values were corrected by using Kraus'[32] approach.

Solvent Imaging. The cured samples were swollen in cyclohexane and were imaged using the spin-echo pulse sequence at 300 K. The intensities of the mobile protons of the solvent probe the homogeneities and spatial distribution of the cross-linked network systems. Areas of low solvent concentration can be correlated with higher cross-link density; similarly, areas of high solvent concentration can be correlated with lower cross-link density. The imaging experiment is essentially a two-dimensional swelling experiment.

The nonuniformity of the signal indicates that a system under investigation has an inhomogeneous cross-link distribution. The color scale used in the displayed images is from 0 to 255 corresponding to from blue to red. The lighter (blue) area represents the lowest signal intensity, while the red area indicates the high signal intensity. The intermediate level of the solvent signal (i.e., between red and blue) is indicative of intermediate level cross-linking.

The images acquired using the spin-echo pulse sequence are shown in Figures 2–4 swollen in cyclohexane. Parts a–e of Figure 2 represent the conventional formulation cured ranging from 20 to 120 min, respectively. The lower signal intensities shown at the boundaries of these samples correspond to the highly cured area. The circular rings with the different signal intensities may be the result of thermal gradients, leading to reduced mobility of the network structures. A similar kind of trend is found in other images with different formulations. Parts d and e of Figure 2 which were cured at 60 and 120 min, respectively, thus show a relatively high intensity signal area, and one possible explanation is that the sample is undergoing reversion.

Parts a–e of Figure 3 represent the semiefficient formulation. The image in Figure 3a represents a 20-min-cured sample, and the intensity distribution shows regions of a low level of cure. The sample cured using 120 min (Figure 3e) gives the overcure distributions of signal intensities. Similarly, parts a–e of Figure 4 represent the efficient formulation. The inhomogeneous distribution of a high intensity signal along with structural defects can be seen in all these images. The effective pixel resolution is 39 μm/pixel in these images.

Direct Rubber Proton Imaging. The relatively high chain mobility and consequent narrow proton line width of the swollen elastomer allow one to acquire the direct image of the rubber. Representative images of conventional formulation are shown in Figure 5. These images were acquired using deuterated cyclohexane as the swelling agent. Inhomogeneities, like spatial defects, voids, and the domains of high cross-link density, make up the bulk of the samples. The inhomogeneities arise from the magnetic susceptibility differences.

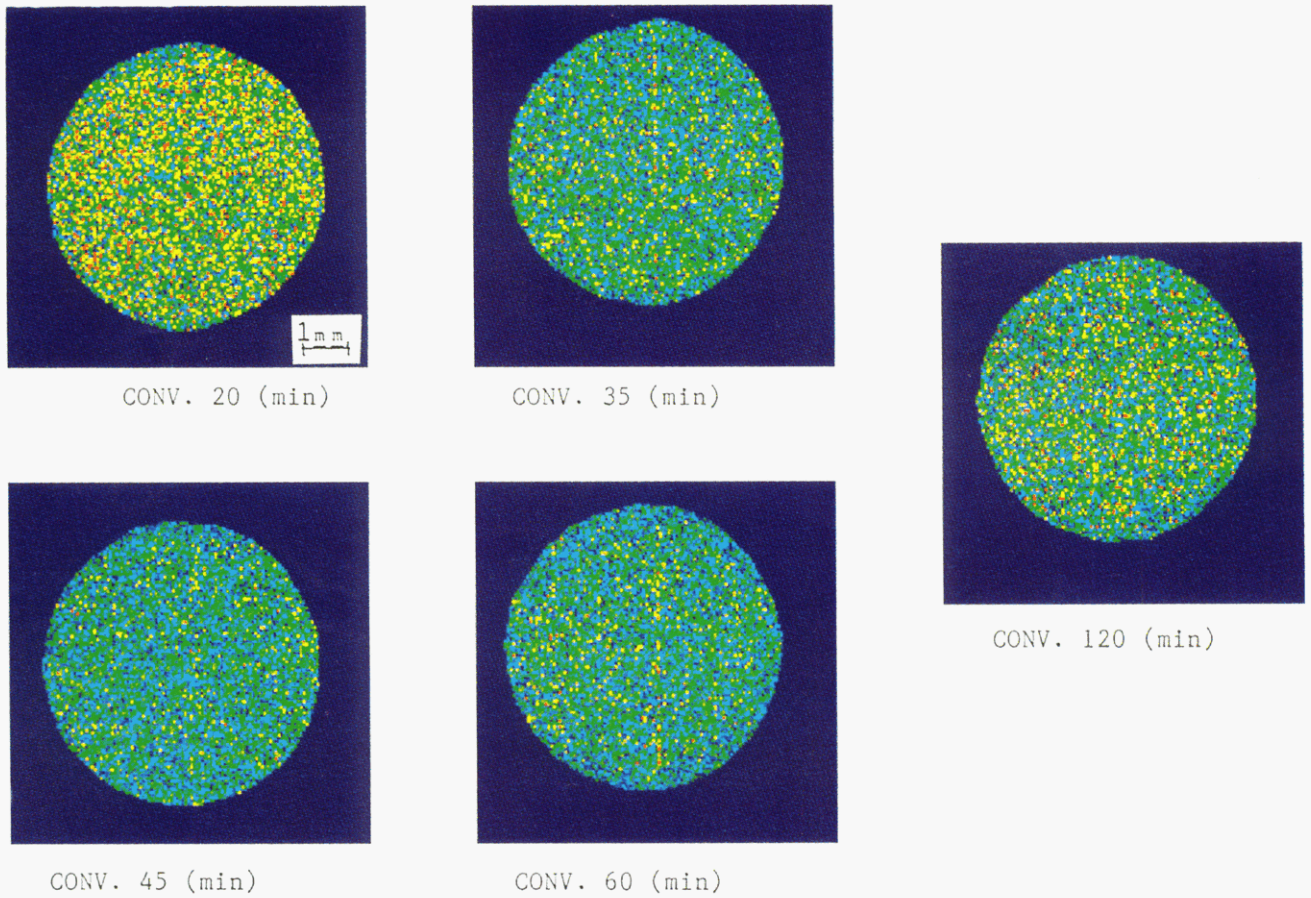

Figure 5. Proton image of a high-vinyl polybutadiene cured sample swollen in deuterated cyclohexane using spin-echo pulse sequence. FOV = 9 × 9 mm displayed as 256 × 256 pixels. The effective pixel resolution is 32 μm/pixel. (a) 20 min; (b) 35 min; (c) 45 min; (d) 60 min; (e) 120 min cured (conventional formulation).

Parts a–e of Figure 5 represent the conventional formulation cured between 20 and 120 min. All these figures are displayed as a gray level cut at 150° and the corresponding intermediate- to high-intensity signal. In the case of Figure 5a which is a 20-min-cured sample, the distribution of high signal intensity can be differentiated from the other images. The differences presumably are based on T_2 differences which decrease with an increase in cross-links. On the other hand, the image shown in Figure 5e gives the high-intensity signal because of possible reversion or chain scission reactions. A similar kind of trend is observed in sev and ev formulations. The effective pixel resolution in these images is 32 μm/pixel.

***T*$_1$ Imaging.** Representative spin–lattice relaxation (T_1) images are shown in Figure 6 corresponding to the ev formulation. These images are displayed as 256 × 256 pixels with an effective resolution of 32 μm/pixels. A T_1-weighted image was calculated using in-house software written[34] in FORTRAN 77.

For T_1-weighted images the contrast within the image is dependent on the polymeric material's characteristic T_1 values. The best TR value depends upon the T_1 of the polymer being imaged. The slight increase in the high-intensity signal with the cross-link densities is probably due to the contribution of short T_1 components.

Discussion

The spatial inhomogeneities present in these samples are the result of different factors, e.g., poor mixing of different ingredients, large thermal gradients, the presence of small foreign particles, and chemical shift and susceptibility artifacts (Figures 2–4).

Inhomogeneities of various sizes and shapes can be seen throughout the bulk of the sample. The portion of the images represented by an intermediate signal (yellow–green) has an intensity corresponding to an intermediate level of cross-linkings. Abrupt changes in magnetic susceptibility at defect interfaces can create shape and intensity artifacts in NMR images.[35,36] Another source of inhomogeneities may be due to the presence of interfaces between the diamagnetic rubber and unmixed paramagnetic materials.

Figure 4d is an image of a sample cured 60 min which shows more areas corresponding to low intensity or the high cross-link density region. The 20-min-cured sample having a conventional formulation is shown in Figure 5a and gives higher intensity signals as compared to the samples with 35-, 45-, and 60-min cure. The exception is the 120-min cure resulting from reversion or overcure reactions. The high-intensity region is due to the presence of mobile proton fractions in the sample.

The NMR image is generally characterized by three factors: (a) spatial resolution, (b) object-contrast level, and (c) its signal-to-noise ratio (S/N). The decrease in the S/N after the maximum cure time may be due to the lowering of the sulfur level or decrease in cross-links. Going through the maximum and then decreasing with additional cure time is not likely due to the loss of network structure by reversion. The reversion reaction normally occurs when the desulfurization reactions are faster than the cross-link reactions. The desulfurization can also follow other pathways in which the species decomposes into conjugated chains, cyclic sulfides, shorter sulfur links, and other main-chain modifications.

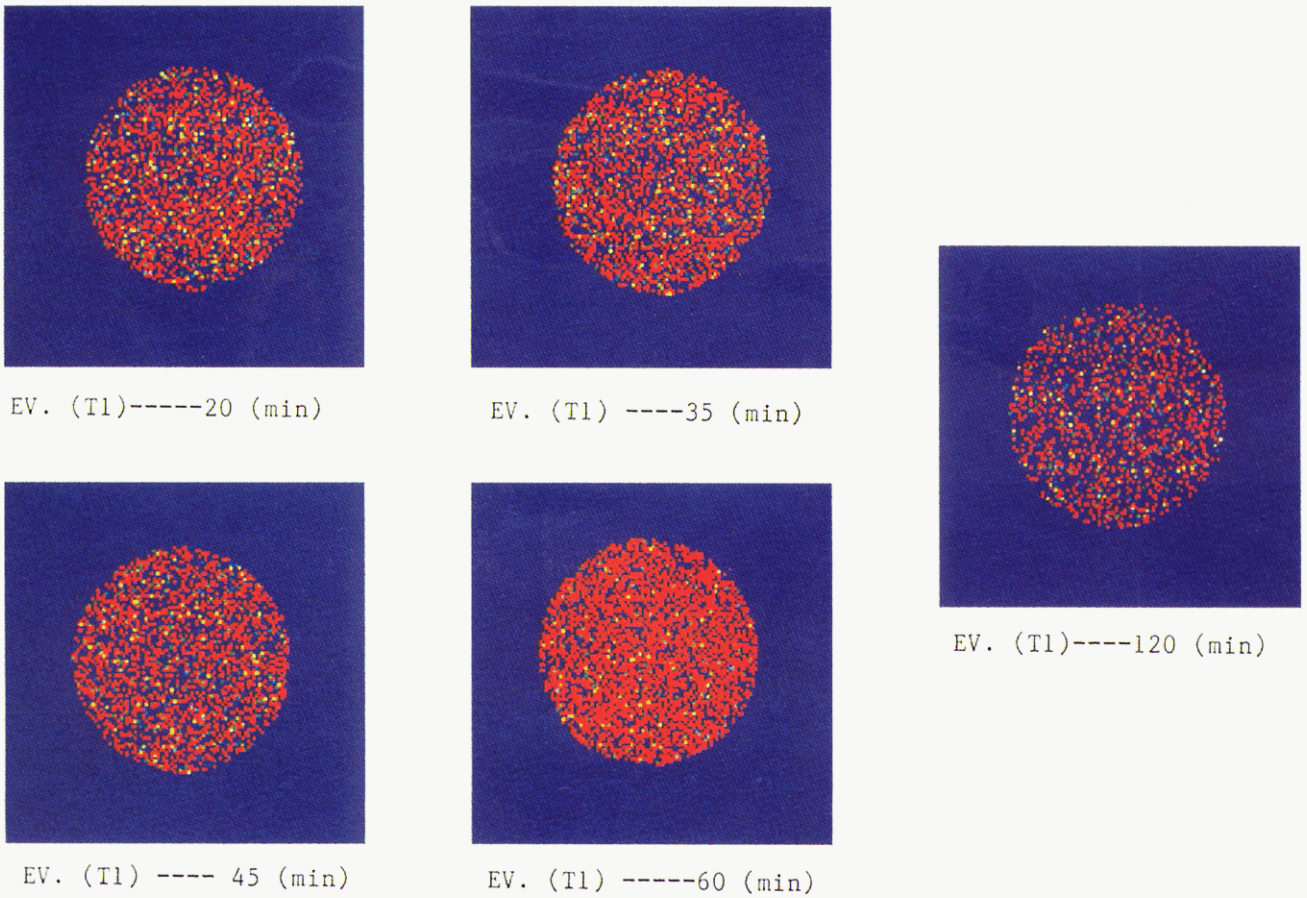

Figure 6. T_1-weighted images of an efficient formulation cured at different cure times using inversion–recovery pulse sequence.

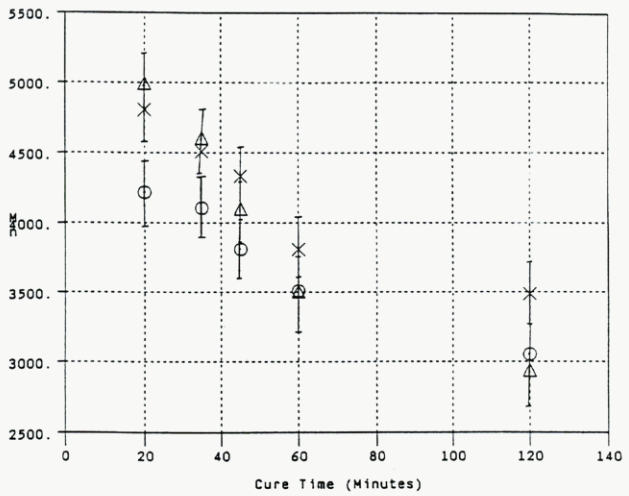

Figure 7. Experimental $M_{n,phys}$ versus cure time at 150° using the equilibrium swelling method: (○) conv; (×) sev; (△) ev.

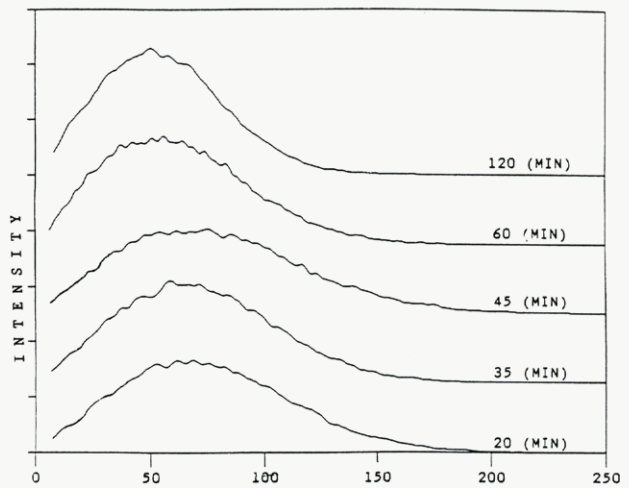

Figure 8. Histogram of the number of pixels corresponding to a particular intensity of the images shown in parts a–e of Figure 5 having conventional formulation.

A graphical representation of $M_{n,phys}$ calculated (using the equilibrium swelling method) versus the cure time is given in Figure 7. The decrease in $M_{n,phys}$ as a function of cure times is due to the decrease in the number-average molecular weight between the cross-links. The study of accelerated–sulfur cured high-vinyl BR demonstrated the existence of correlation between swelling-measured cross-link densities and the intensities associated with it.[37]

A histogram of the number of pixels with a particular value of T_2 versus T_2 can be interpreted in terms of the distribution of cross-links along the chain. Figure 8 shows the different histograms for a conv system. The peak maxima are shifted to the left in all these samples. Also shown is a narrowing of the distribution of the cross-link densities as we move from low to high cure times. In other words, the probability of finding the molecules with lower mobility (cross-linked) becomes greater for an efficiently cured system.

The histogram intensity corresponding to the gray level cut at 200° (red color) is plotted as a function of cure times (Figure 9). The intensity decreases gradually from 20- to 60-min cure but starts to increase for the sample with 120-min cure and is probably a result of reversion reactions. Similarly, the histogram intensities cut at 170° (arbitrarily selected) on a gray scale (yellow color = intermediate cross-link level) are plotted against cure times and give the same trend as shown in Figure 10.

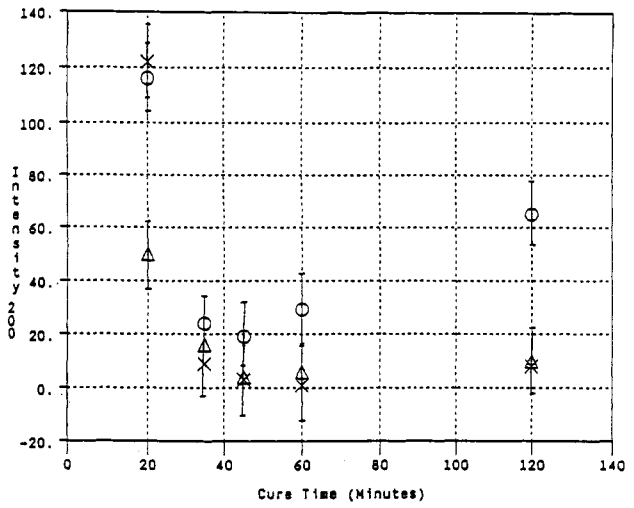

Figure 9. Plot of histogram intensity versus cure time for all three formulations. The gray level cut at 200° on the scale of 0–255: (○) conv; (×) sev; (△) ev.

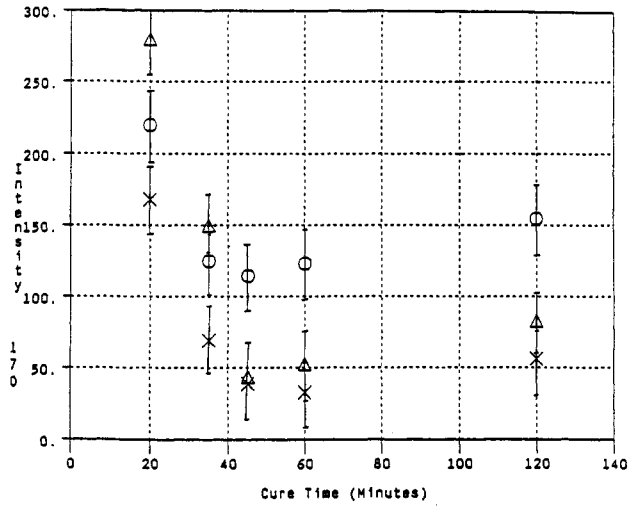

Figure 10. Plot of histogram intensity versus cure time for all three formulations. The gray level cut at 170° on the scale of 0–255: (○) conv; (×) sev; (△) ev.

Table 4. Tabulation of Histograms Shown in Figure 8 (Conv)

cure time (min)	av value	median	stand dev	skewedness	kurtosis
20.0	78.8	99.0	39.1	5.7	-3.1
35.0	75.5	94.1	36.6	5.2	-2.5
45.0	71.5	87.8	33.3	4.9	-1.8
60.0	63.0	80.0	31.6	3.8	-1.0
120.0	56.0	69.8	26.7	1.7	1.9

standard deviation: ±0.11

Table 4 shows the calculation of the histograms for conventionally cured samples displayed in Figure 8. The average, median, and standard deviation values are described in Table 4. The standard deviation is calculated for these histograms, and it decreases from low to high cross-link density, indicating a narrowing of the distributions. The skewedness and kurtosis of these histograms have also been calculated. The proton NMRI T_1 data was analyzed assuming the presence of only one component (an exponential function). The samples were prepared using the cure time ranging from 20 to 120 min. All these images were taken in deuterated cyclohexane. In the case of T_1-weighted images of the efficient formulation (Figure 6), the high-intensity signal increases from 20- to 60-min cure and then decreases. The rationale behind this process is the desulfurization after a certain level of cure.

Table 5. Percent Area of High- and Low-Intensity Signals of the Images Shown in Figures 2–4

	cure time (min)				
cut level[a]	20	35	45	60	120
conv					
un-cross-linked	85.5	89.6	68.1	70.5	24.6
cross-linked	10.5	7.3	25.9	25.8	68.1
voids	4.0	3.1	6.0	3.7	7.3
sev					
un-cross-linked	96.1	26.5	28.5	38.4	23.7
cross-linked	2.8	69.3	67.7	59.0	69.6
voids	1.1	4.2	3.8	2.6	6.7
ev					
un-cross-linked	89.4	25.6	23.8	55.3	22.3
cross-linked	6.8	65.5	70.8	40.8	72.1
voids	3.8	8.9	5.4	3.9	5.6

error: ±5.0%

[a] Values are cut for un-cross-linked at 220°, cross-linked at 100°, and voids at 150° on the scale of 0–255 of histograms.

Similar trends were found in conventional and semiefficient formulations. In sev the intensity increases from 35 to 60 min and decreases at 120 min. As the curing proceeds from a conventional to an efficient system, there is an increase in the molecular rigidity which is reflected in a reduction of the T_1 and T_2 of the proton. Besides enabling detection of the size and location of voids and structural defects in a rubber sample by visual observation of the images, NMRI methods can be made to yield numerical evaluation of the void size and fraction of voids in a sample.

Table 5 shows the percent areas of the images cut at 220° (lightly cross-linked regions) and 100° (high cross-link regions) as displayed in Figures 2–4. The percent area corresponding to voids is cut at 150° on the scale of 0–255. The resolution of the microimaging probe in this case is 0.07 mm. With the exception of a few large morphological defects, the spin-echo image appears uniform but mottled.

Conclusions

^{1}H imaging reveals the different physical and spatial microstructures present in an unfilled accelerated–sulfur cured high-vinyl polybutadiene. Advantages of this technique are its nondestructive nature and the abundance of detectable molecular parameters including molecular motions.

Voids and nonvoids can be differentiated based on magnetic susceptibility differences. Morphological defects and the areas corresponding to different cross-link densities are detected using a solvent imaging method. Cyclohexane was used as a solvent to act as a physical probe. The swelling measurements method based on Flory–Rehner's equation was also employed to determine the cross-link densities and number-average molecular weights between the cross-links as a function of cure times. Nonuniform signal intensities and T_2 times within the swollen high-vinyl polybutadiene network material indicate inhomogeneities on the order of tens of microns.

The images acquired in cyclohexane demonstrate a different cure pattern in these samples. The high cross-link regions are present adjacent to the mold, which indicates that it is thermal gradient driven. The sample cured for 120 min shows greater solvent intensities, demonstrating reversion reaction, and this reversion or overcure reaction also results in spatial inhomogeneities. The inhomogeneities may arise from poor mixing and residual auxiliary agents. The percent areas corresponding

to un-cross-linked, highly cross-linked, and void regions are calculated using a contour imaging method.

T_1-weighted images were also calculated for the three formulations. These intensities are relatively less affected with the progress of vulcanization. The contrast between the different regions is due to proton density and T_1-weighted images, suggesting that the variation seen in the images may be closely related to the variation in both concentration and the mobility of the network systems.

Acknowledgment. The authors acknowledge Monsanto Corp., Akron, OH, for their technical support of this research. Also the author expresses his thanks to the National Science Foundation for support of Grant No. DMR92-24176.

References and Notes

(1) Mansfield, P.; Morris, P. G. *Adv. Magn. Reson.* **1982**, Suppl. 2.
(2) Gummerson, R. J.; Hall, C.; Hoff, W. D.; Hawkes, R.; Holland, G. W.; Moore, W. S. *Nature (London)* **1979**, *281*, 56.
(3) Koenig, J. L. *Spectroscopy of Polymers*; American Chemical Society: Washington, DC, 1992.
(4) Komoroski, R. A., Ed. *High Resolution NMR Spectroscopy of Synthetic Polymers in Bulk*; VCH Publishers: Deerfield, FL, 1986.
(5) Andreis, M.; Koenig, J. L. *Adv. Polym. Sci.* **1989**, *89*, 69.
(6) Weisenberger, L. A., Koenig, J. L. *Adv. Polym. Sci., Part C: Polym. Lett.* **1989**, *27*, 55.
(7) Persson, S.; Ostman, E. *Appl. Opt.* **1985**, *24* (23), 4095.
(8) Persson, S. *Polymer* **1988**, *29*, 802.
(9) Liu, J.; Nieminen, A. O. K.; Koenig, J. L. *Appl. Spectrosc.* **1989**, *43* (7), 1260.
(10) Clough, R. S.; Koenig, J. L. *Adv. Polym. Sci., Part C: Polym. Lett.* **1989**, *27*, 451.
(11) Smith, S. R.; Koenig, J. L. *Macromolecules* **1991**, *24*, 3496.
(12) Rothwell, W. P.; Gentempo, P. P. *Bruker Report* **1985**, *1*, 46.
(13) Rothwell, W. P.; Holecek, D. R.; Kershaw, J. A. *Adv. Polym. Sci., Part C: Polym. Lett.* **1984**, *22*, 241.
(14) Hall, L. D.; Rajanayagam, V. *J. Magn. Reson.* **1987**, *74*, 139.
(15) Mansfield, R. A.; Grannel, P. K. *Phys. Rev. B* **1975**, *12*, 3618.
(16) Wind, R. A.; Yannoni, C. S. *J. Magn. Reson.* **1979**, *36*, 269.
(17) Szeverenyi, N. H.; Maciel, G. *J. Magn. Reson.* **1984**, *60*, 460.
(18) Emid, J.; Creyghton, J. H. N. *Phys. Rev. B* **1985**, *128*, 81.
(19) Suits, B. H.; White, D. *J. Appl. Phys.* **1986**, *60*, 3772.
(20) Corey, D. J.; Van Os, J. W. M.; Veeman, W. S. *J. Magn. Reson.* **1988**, *76*, 543.
(21) MacDonald, P. J.; Attared, J. J.; Taylor, D. G. *J. Magn. Reson.* **1987**, *72*, 224.
(22) Miller, J. B.; Garroway, A. N. *J. Magn. Reson.* **1989**, *77*, 187.
(23) Cory, D. J.; deBoer, J. C.; Veeman, W. S. *Macromolecules* **1989**, *22*, 1618.
(24) Chang, C.; Komoroski, R. A. *Macromolecules* **1989**, *22*, 600.
(25) Cottrell, S. P.; Halse, M. R.; Strange, J. H. *Meas. Sci. Technol.* **1990**, *1*, 624.
(26) Jezzard, P.; Carpenter, T. A.; Hall, L. D.; Jackson, P.; Clayden, N. J. *Polym. Commun.* **1991**, *32* (3), 74.
(27) Cory, D. J.; Gravins, S. *Materials Research Society Conference*, Boston, MA, 1990.
(28) McBrierty, V. J.; Douglass, D. C. *J. Polym. Sci., Macromol. Rev.* **1981**, *16*, 295.
(29) Carr, H. Y.; Purcell, E. M. *Phys. Rev.* **1954**, *94*, 630.
(30) Meiboom, S.; Gill, D. *Rev. Sci. Instrum.* **1958**, *29*, 688.
(31) Flory, P. J. *J. Chem. Phys.* **1950**, *18*, 108.
(32) Kraus, G. *J. Appl. Polym. Sci.* **1963**, *7*, 1257.
(33) Moore, G. C.; Watson, W. F. *J. Polym. Sci.* **1956**, *19*, 237.
(34) Liu, J.; Nieminen, A. O. K.; Koenig, J. L. *J. Magn. Reson.* **1989**, *85*, 95.
(35) Chu, S. C. K.; Xu, Y.; Balschi, J. A.; Springer, C. S. *Magn. Reson. Med.* **1990**, *13*, 239.
(36) Ludeke, K. M.; Roschman, P.; Tischler, R. *Magn. Reson. Imaging* **1985**, *3*, 329.
(37) Rana, M. A.; Koenig, J. L. *Rubber Chem. Technol.* **1993**, *66* (2), 242.